Hindawi
Geofluids
Volume 2022, Article ID 1592703, 19 pages
https://doi.org/10.1155/2022/1592703

Research Article

Deformation and Failure Process of Slope Caused by Underground Mining: A Case Study of Pusa Collapse in Nayong County, Guizhou Province, China

Shaozhen Xiong,[1] **Wenbing Shi**,[1,2,3] **Yong Wang**,[1,3] **Chun Zhu**,[4] **and Xiaoxiao Yu**[1]

[1]*College of Resource and Environmental Engineering, Guizhou University, Guiyang 550025, China*
[2]*Key Laboratory of Karst Geological Resources and Environment, Guizhou University, Guiyang 550025, China*
[3]*Mountain Geohazard Prevention Research and Development Center of Guizhou Province, Guiyang 550025, China*
[4]*School of Earth Sciences and Engineering, Hohai University, Nanjing 210098, China*

Correspondence should be addressed to Wenbing Shi; wbshi@gzu.edu.cn

Received 19 April 2022; Accepted 4 July 2022; Published 10 August 2022

Academic Editor: Guang-Liang Feng

Pusa village is located in the karst mountain area of Nayong County, Guizhou Province, China. Laoyingyan mountain rock is gently dipping, the upper part consists of hard rock formations, and the lower part is made up of soft rock composed of 3 coal seams. On August 28, 2017, a massive landslide occurred in this area, resulting in 82,3000 m^3 of debris, which resulted in significant casualties and brought up the malaise in society. In this paper, the geological conditions and long-term mining activities in the study area are analyzed by field investigation. The base friction tests and numerical models are used to simulate and analyze the failure and deformation process of Pusa collapse to accommodate the research on the deformation and failure mechanism of the slope and provide better prevention and treatment suggestions. The results show that the Pusa collapse can mainly be attributed to unique geological conditions, underground mining activities, and the topography of the slope. The intensified mining activities promoted the development of fractures and cracks in the slope, resulting in unstable upper slopes. The failure process of the Pusa collapse can be summarized into four-stage: the development of goaves roof deformation, the crest of the slope cracks, intensification of deformation, and occurrence of collapse. The upper slope with high strength rock developed crack-toppling failure. Meanwhile, the upper slope with low strength rock developed subside-crack-sliding failure, and those two failures together contributed to the mechanism of Pusa collapse. Slope deformation and failure mechanism can be summarized as subside-crack-toppling-shear sliding type.

1. Introduction

Geohazards, such as rockfalls, rock avalanches, landslides, debris flows, and ground collapse, are driven by adverse geological features [1], global climate changes [2], and/or unscientific human activities [3]. Geohazards are considered the second most destructive natural disaster after earthquakes [4]. The geohazards lead to increasing threats as more people and property are exposed to them than ever [5]. The mining-induced landslides and rock avalanches have attracted growing public attention among geological hazards [6]. Many landslides and rock avalanches are reported to regard to the impact of the underground mining activities, such as Huang et al. [7], Xu et al. [8], Wu and Kulatilake [9], Jiao et al. [10], Kulatilake and Ge [11], Zhao et al. [12], Fan et al. [13], and Zhu et al. [14]. These geological disasters share the characteristics of large-scale, strong suddenness, and complex causes. Their occurrence will cause heavy casualties and property losses.

Underground mining activities may alter the stability of slopes [15]. The surface movement characteristics induced by underground mining in mountainous areas are considerably different from those caused by slope excavation or open-pit mining [16–18]. The surface movements may cause subsidence, slope movements, discontinuous deformations,

and variation in hydrogeological conditions [19]. Slope movements can potentially convert into slope failures such as slides, rockfalls, rock avalanches, and debris flows under unfavorable conditions [20–23]. There are four main reasons for slope failure caused by underground mining: (1) stress redistribution and the consequent changes in mining slope, (2) changes of physical and mechanical properties of the slope, (3) generating internal and surficial cracks due to overburden rock mass deformation in mining area, and (4) changes of hydrological actions of the slope accelerate the slope deformation and failure [24].

Rock avalanches are slope process detachments that refer to sliding, toppling, or falling [25]. It is commonly believed that underground mining has a cantilever effect on the layered rock, which leads to the destruction of overburdened rock and ground cracks [26–28]. Rock avalanches associated with underground mining have been reported throughout mining history. Many studies have improved understanding of ground movement, and the instability of the slopes related to overburdened strata stress changes in recent years [29–31]. It is crucial to understand the mechanism of deformation and failure of gently sloping slopes and the stability of underground mining [12]. Significant progress has been made on analyzing mining-induced geohazards using numerical simulations, physical modeling tests, and geomechanic analyses. [32].

Currently, numerical simulations such as finite element and discrete element methods are widely used for assessing geohazards worldwide [33, 34]. Numerical methods can consider complex underground excavation geometries, topography, and geological conditions. It is an excellent method to deal with nonlinear behaviors of rock mass, whose deformation process can be replicated with numerical tools [35]. In particular, the discrete element method (DEM) based on the formulation and solution of equations of motion of rigid and deformable bodies has a broad application in rock mechanics, including rock dynamics, lab test simulation, rock slopes, geohazards, and underground mining [36]. The most representative explicit DEM methods are the UDEC, PFC, and 3DEC for 2D and 3D problems in rock mechanics, which are widely used to study slope deformation and destruction mechanisms. Cruden and Martin [37] analyzed the formation lithology, geological structure, displacement, and deformation characteristics of the Frank landslide through a geological survey. Marschalko [38] and others [39] analyze a large number of monitoring data that the picking directly impacts slope deformation, especially in the upper part of the mining area caused by subsidence. Benko and Stead [40] used numerical models to study the effects of different mining methods, mining depths, and tectonic features on slope deformation damage. The physical model is also an essential approach for investigating the mechanism of slope deformation destruction. Zheng et al. [32] used a physical model to analyze the collapse damage process and destruction patterns. It can be seen that numerical methods such as FEM and DEM become prevalent in studying the mechanisms of slope deformation destruction.

Pusa avalanche occurred in Pusa village, Zhangjiawan Town, Guizhou Province in southwest China on August 28, 2017, which is about 191 km to the Guiyang city, the capital of Guizhou Province (Figure 1). It is located in the southern working district of the Pusa mine in an area affected by underground mining. The collapse volume was about 500,000 m^3, destroying a part of Pusa village causing 35 deaths [13]. After the avalanche, approximately 1,000,000 m^3 of bedrock debris flow buried some houses of the Pusa village at the toe of the escarpment. Significant casualties and social impacts were recorded [14].

Many achievements have been made in researching slope deformation and instability mechanisms. Still, the research on the internal mechanism of high and steep slope deformation and failure is relatively limited. In this paper, Pusa village is selected as a research case. Combined with field investigation and geological data, the geological engineering conditions, influential factors of collapse formation, slope deformation and failure characteristics, and essential collapse attributes in the study area were analyzed. To study the deformation and failure mechanism of high and steep slopes under underground mining, a physical modeling method is adopted to reproduce the whole process of collapse from incubation to occurrence, and a numerical method is adopted to simulate and verify the failure mechanism of the slope. Based on the analysis and discussion, a theoretical basis was proposed to study the deformation and instability mechanism of such a slope.

2. Geological Conditions and Mining Activities

2.1. Geomorphology. The study area is located in the second step of Yunnan Guizhou Plateau—Qianxi mountain plain, which belongs to Wumeng Mountain erosion landform. The overall terrain of the site is high in the south and low in the north. The highest elevation point of Laying mountain is 2175 m, and the lowest is 1875 m and is located at the ditch of Pusa village at the lower part of the slope. The relative elevation difference is about 300 m, and the slope gradient is 10°-25°. The slope gradient of some sections can reach 55°. The upper part of the research area (Laying mountain) is a cliff, and the lower part is a gentle slope, with an elevation difference of about 200 m (Figure 2). The lower coal measure strata are coal-bearing strata of the Longtan Formation of the Upper Permian system. The terrain at the outcrop is gentle. The general elevation is between 1700 and 1900 m, and the average height is about 1850 m. Most of the area is covered by a quaternary system, mainly farmland and housing land. The precipitation range in the study area is 1200-1300 mm, and the average annual precipitation is 1238.8 mm. According to rainfall data recorded by Guizhou's local meteorological bureau, the total rainfall in August 2017 was only 44.3 mm.

2.2. Lithology and Geological Structure. The Pusa avalanche was located in the southeast wing of the Zhangwei anticline. The Pusa slope face dip is located at NW50°, with an average slope angle of 40-55°. It also has two fee faces at NE40° and SW80°, respectively, with an average slope angle of 50-65°. The bedding plane is 280°∠8° – 10°. There are three major fault systems F1, F2, and F3 developed. However, no connection between fault and collapse can be recognized. Through the field survey, three major joint sets (J1, J2, and J3) are

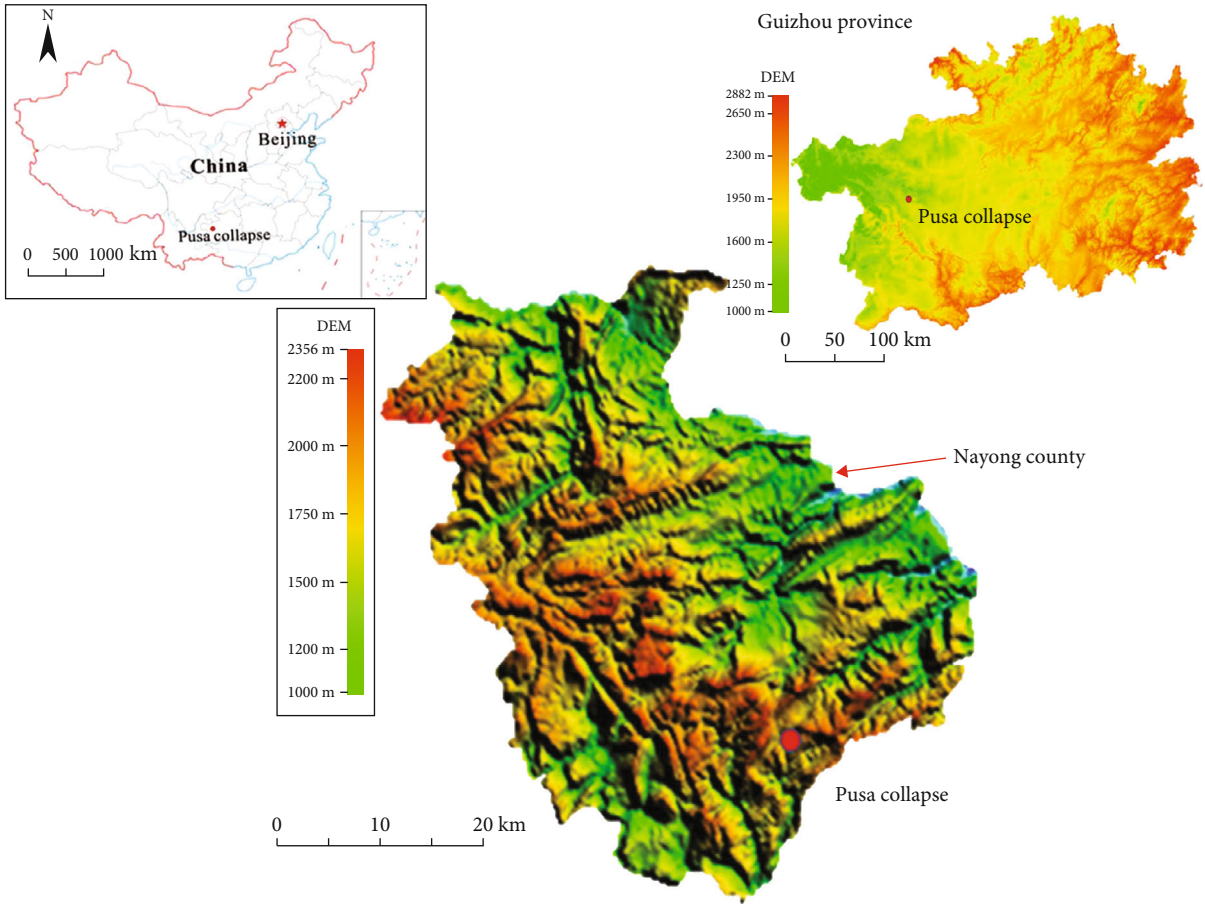

Figure 1: The location picture of Pusa collapse, Nayong county of Guizhou province.

identified in the area. J1 joints set presents at N50°-60° E/∠80-90°, J2 at N81-84° W/∠80-90°, and J3 at N10-15° E/∠80-90°. These joint sets result in rock mass into blocks. The combination of joint sets and bedding planes is one of the dominant factors of the Pusa avalanche. The typical strata sequence in the area ranging from new to old are as shown in Figure 3.

(1) *The Yelang Formation of the Lower Triassic (T_1y).* Limestone, sandy mudstone, and argillaceous sandstone. According to lithology and age, Yelang Formation can also be classified into two stages: T_1y^1 and T_1y^2. T_1y^1 consists of thin-medium layered limestone, forming a cliff in the upper part of the study area. T_1y^2 consists of sandy mudstone and argillaceous sandstone, forming a steep slope in the middle and lower area

(2) *The Changxing-Dalong Formation (P_{3c+d}) of the Upper Permian.* Medium-thick layered argillaceous limestone

(3) *The Longtan Formation (P_3l) of the Upper Permian.* Interbedded thin to medium-thick layered sandstone and thin layered siltstone, underlain by 1-2 m thick coal seam

Nayong County was known for its high-quality coal. The minable coal seams are M6, M10, M14, M16, M18, and M20 layers. In descending order, three seams of coal were mined before the collapse, M16, M14, and M10. Underground mining had been carried out for a long time. Illegal and small-scale mining activities were reported to be operated by residents. However, these activities have been banned since1990s. Large-scale mining activities have been carried out since 1995. The location of the coal seam is shown in Figure 3.

The large-scale mining activities were mainly classified into two stages: production scale of 60,000 tons/year (between 1995 and 2010) and 300,000 tons/year (2011-present). The dip angle of M16, M14 and M10 coal seams is 7°, and the roof rock is powder sandstone and powder sand mudstone. The thickness of the M16 coal seam is 1.20-2.04 m, with an average of 1.60 m. Mining in M16 was utterly stopped in December 2010. The M14 is mined from 2013 to the second quarter of 2016 with an average layer thickness of 1.23 m, and the M10 is mined from 2016 to August 2017 with an average layer thickness of 2.12 m. By June 2016, the M10 coal seam had been mined. M10 was mining out before the Pusa avalanche occurred.

3. Characteristics of Pusa Collapse

3.1. Signs of Slope Deformation. According to the geological data collected before the collapse, the residents' description, and the image data, the historical deformation process of the Pusa collapse was preliminarily understood.

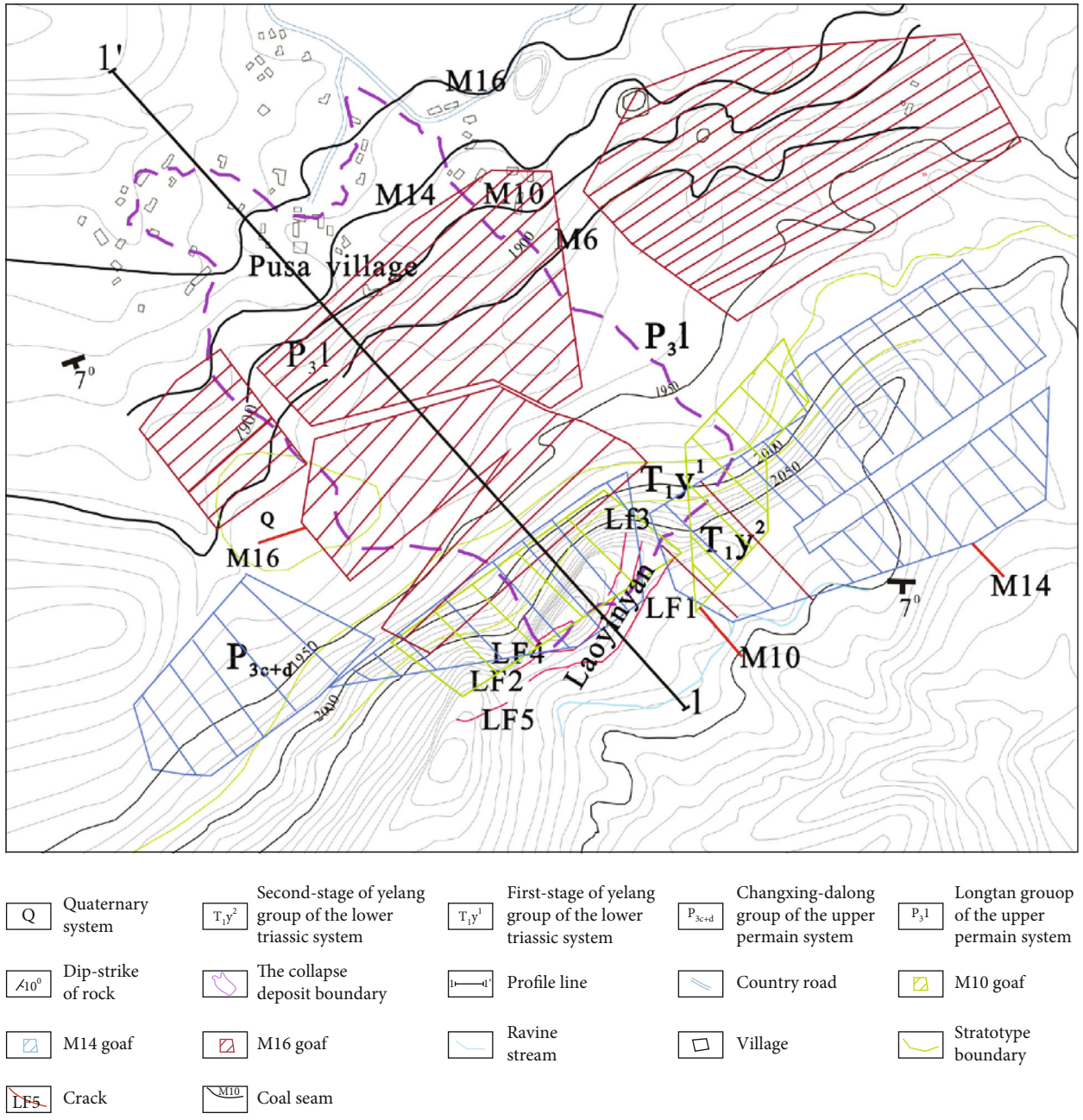

Figure 2: Regional topographic and geological map of Pusa collapse.

The deformation of the slope could be summarized as follows:

(1) There were minor signs of deformation at the top of eagle rock mountain and small cracks in 2006. These tiny cracks gradually developed and expanded

(2) Till 2013, a considerable number of long, wide cracks had already existed at the back of the Laoyingyan mountain. Among them, the width of the crack denoted as Lf1 was about 1–2 m, and the crack extended up to 215 m, which constituted the boundary of the whole mountain body that deformed. Lf2 and Lf3 were located at the back border of the collapse source area, and there were signs of further deformation. It can be seen a small, localized collapse occurred near another mountain on the south side of the slope (of which the estimated volume of about 3×10^3 m^3) and that the collapsed debris accumulated on the slope surface (Figure 4(a))

(3) In 2014, compared with cracks in 2013, Lf3 extended and connected with some small fractures with a length of 179 m. The width of the cracks found elsewhere on the collapsed slope also reached 40 cm, and the crack width is increasing every year. It was worth

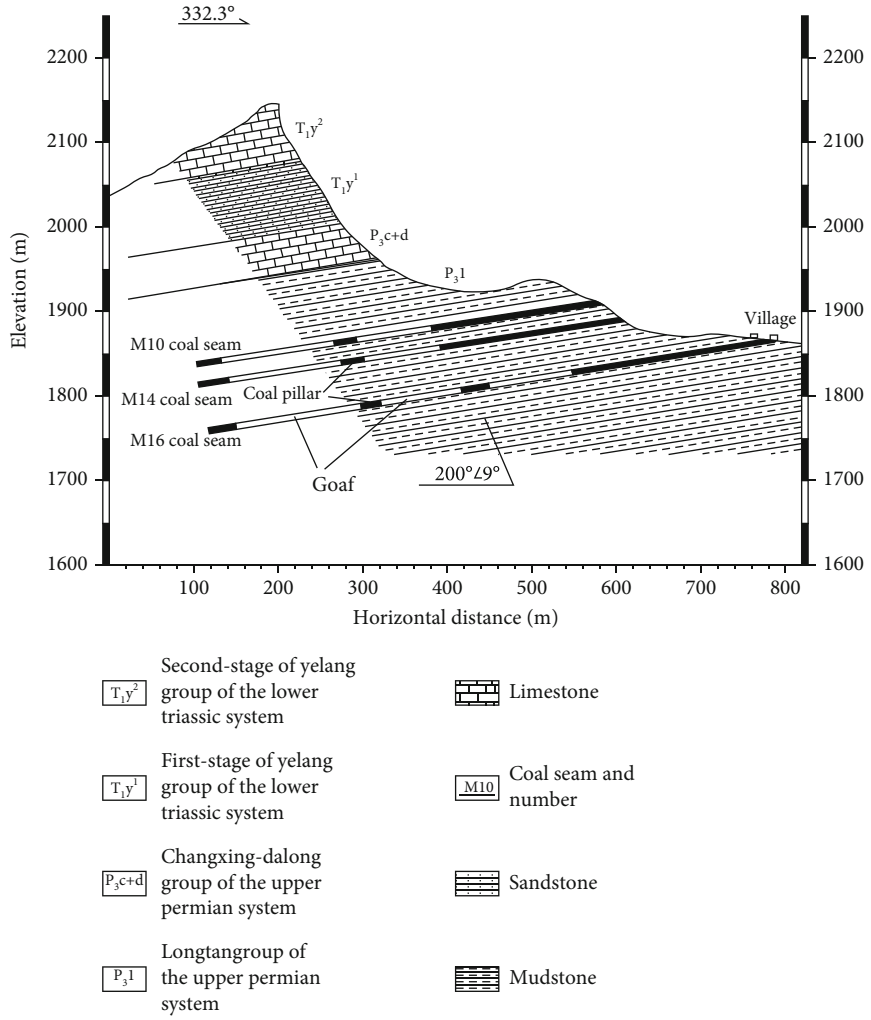

Figure 3: Typical cross-section of the slopes in the site (Profile I-I′ as shown in Figure 2).

noting that there have been several small local collapses on the left side of the source area of the collapse, and the accumulation has increased (of which the estimated volume of about 5×10^3 m^3), which further indicates that the slope has undergone gradual deformation (Figure 4(b))

(4) In 2016, due to the superposition of heavy rainfall and mining, large-scale gravel and clay collapse occurred on the right side of the collapse source area, covering previous collapse accumulations and blocking roads (Figure 4(c))

(5) In July 2017, several collapses occurred in Laoyingyan mountain, and the slope also fell from time to time

(6) On August 28, 2017, Pusa collapse occurred, and the rear side of Laoyingyan mountain had prominent subsidence characteristics, which was stepped. The rock mass at the top of the mountain was incredibly broken, and there were many tensile fractures, among which Lf1 extends to 180 m and width was 34 m (Figure 4(d))

Combined with the macrodeformation of the slope in each period, the slope deformation can be summarized as slow deformation-rapid deformation-collapse. In the early stage, the deformation of the mountain is slow, the slope is intact, and there are only some tiny cracks. Then, the deformation intensifies, with many small collapses occurring, and the cracks become longer and broader. The deformation of the collapse source area is severe and continuous, and rockfall often occurs on the slope. Finally, the continuous deformation makes the mountain collapse. The development of cracks and voids on the three sides of the slope is disadvantageous of the slope collapse, which provides geometric conditions for slope failure.

3.2. Characteristics of Collapse Failure. After the collapse, the collapsed body moved in the direction of 300-310° in debris flow and accumulated at the front edge of the slope foot. The elevation of the rear edge of the steep collapse wall was about 2120 m, the height of the slope toe was about 1922 m, and the relative elevation difference was about 200 m. The horizontal length of the collapse direction was about 800-820 m, the horizontal length of the steep slope foot to the

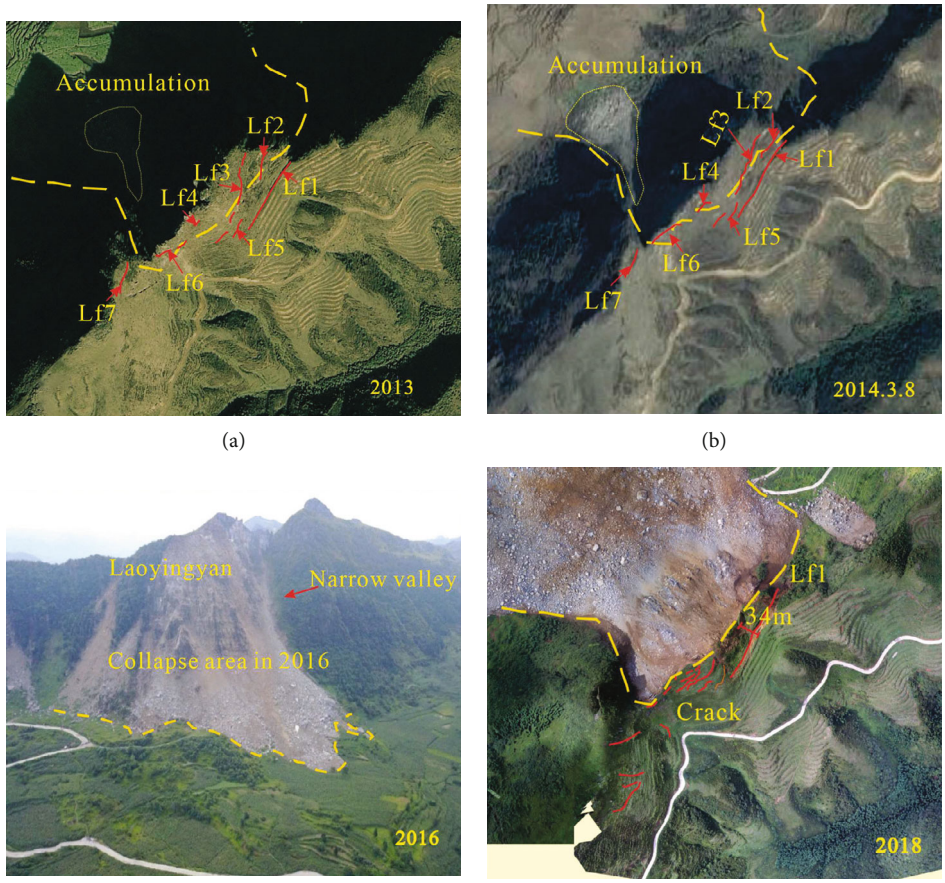

Figure 4: Images of the source area showing the cracks. (a) UAV image, 2013; (b) UAV image, August 2018; (c) front view, July 2016; and (d) UAV image, August 2018. Note: UAV refers to unmanned aerial vehicle.

front edge of the accumulation area was about 660 m, and the average thickness of the accumulation area was about 4 m. The total amount of the collapse was about 82.4×10^4 m^3. According to UAV aerial photography and field investigation, the collapse accumulation was divided into the collapse source area, falling scraping area, and circulation stop area, as shown in Figure 5.

3.2.1. Collapse Source Area. The collapse source area was located in the middle and upper part of the slope. The collapse shear outlet was found in the first member of the Yelang formation of the Lower Triassic system 60-90 m down the slope top (Figures 5(I) and 5(l)). According to UAV aerial photography and field investigation, the average height, width, and thickness of rock mass in the collapse source area were about 85 m, 145 m, and 40 m, respectively. The total volume was about 493,000 m^3.

3.2.2. Falling Scraping Area. After the unstable rock mass suddenly collapses in the collapse source area, it moves downward along the slope under the tremendous gravitational potential energy and kinetic energy. It scraped the surface broken rock mass and slope deposits along the way, and the scrape thickness was about 1.5 m. The scraping area was about 180 m in width and 80 m in height, and the scraping area was about 210,000 m^3 (see Figures 5(II) and 5(a)).

3.2.3. Flow Stop Accumulation Area. The collapse accumulation area was located in the relatively open leading edge of the slow slope area (Figure 5(III)), and the overall slope was about 10-15°. There was a small hill at the front edge of the slope foot. The plane shape of the congeries was irregular fan-shaped, and it accumulated in two directions. The accumulation area was fishtail, with a broad middle part and narrow front and rear edges. The width of the middle part of the accumulation area was about 360-380 m, extending to the SW-NE direction. The accumulation area was scraped by about 310,000 m^3 (see Figures 5(e)–5(h)).

3.2.4. Perturbation Area. With the mining of coal seam, a series of deformation and small-scale collapse has occurred (Figures 5(IV_2) and 5(a)–5(c)). Several small collapses occurred successively on the left side of the collapse source area, and the later collapse accumulation had covered the front collapse accumulation (Figure 5(IV_3)). Many cracks were developed in the disturbed area at the top of the slope (Figure 5(IV_1)). One of the deep cracks was 34 m in width and 180 m in length. The rock mass was broken. The resounding crack separated the collapsed body from the rock

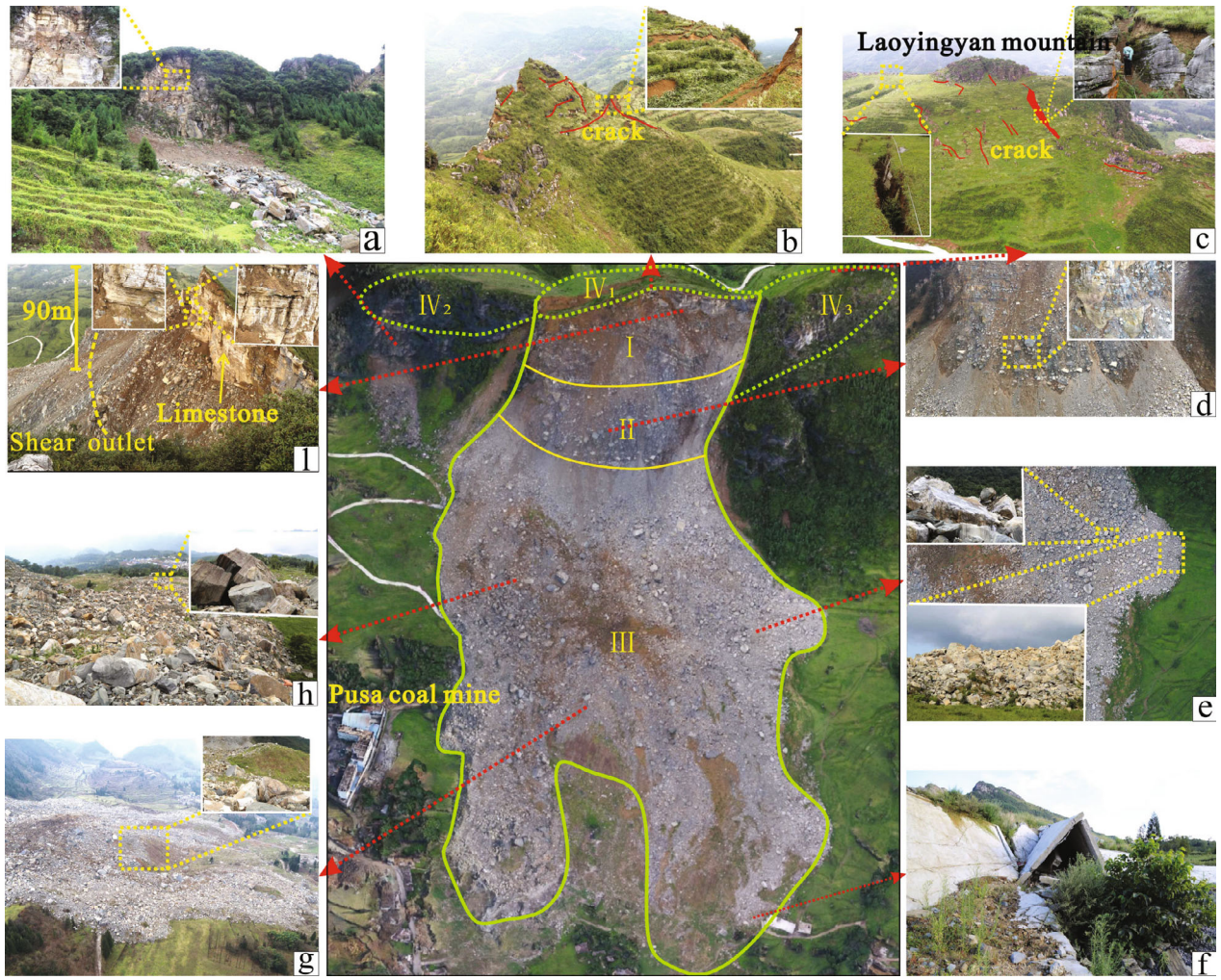

Figure 5: The full picture of the collapse. (I) Collapse source area. (II) Falling scraping area. (III) Flow stop accumulation area. (IV_1) Perturbation area 1. (IV_2) Perturbation area 2. (IV_3) Perturbation area 3.

mass at the back edge. It was possible to slide again under external force.

3.3. Analysis of Collapse Instability Process. When the collapse occurred, the on-site monitoring personnel recorded the whole process of collapse initiation through UAV (Figure 6). By analyzing the video captured by UAV, the starting process of collapse is observed. As can be seen from Figure 6(b), after multiple landslides on the slope, the outward extrusion deformation occurs in the middle of the collapsed body towards the free surface, the rock mass on the suitable surface of the collapsed body begins to fall off, and the cumulative damage occurs in the collapsed body. Then, the collapsed body was deformed violently, and the upper rock mass fell off due to the loss of support of the lower rock mass during outward deformation (Figure 6(c)). Then, the mountain collapses due to toppling deformation, generating tremendous kinetic energy (Figure 6(d)). Finally, the collapsed body develops rapidly and moves downward under the action of gravity. In contrast, the rock mass in the middle and lower part of the collapsed body is scraped by the high-speed debris flow at the top and moves together with the collapse debris flow. At the same time, the whole collapsed body was almost completely transformed into debris flow and slides towards the front edge of the slope at high speed (Figures 6(e) and 6(f)). As the height difference of the whole slope was close to 200 m, the collapsed body had substantial kinetic energy. It moved forward for a long distance, resulting in considerable loss of lives and properties of residents along the travel path.

4. Methodology and Theory

4.1. Method. After the collapse of Pusa, relevant teams and scholars actively exchanged and cooperated, providing valuable information for the research. By analyzing data collected from multiple sources and studying bottom friction test and PFC numerical simulation, this work may contain the first complete overview of landslide events, including deformation and failure process, deformation history, and failure mechanism. Details are as follows.

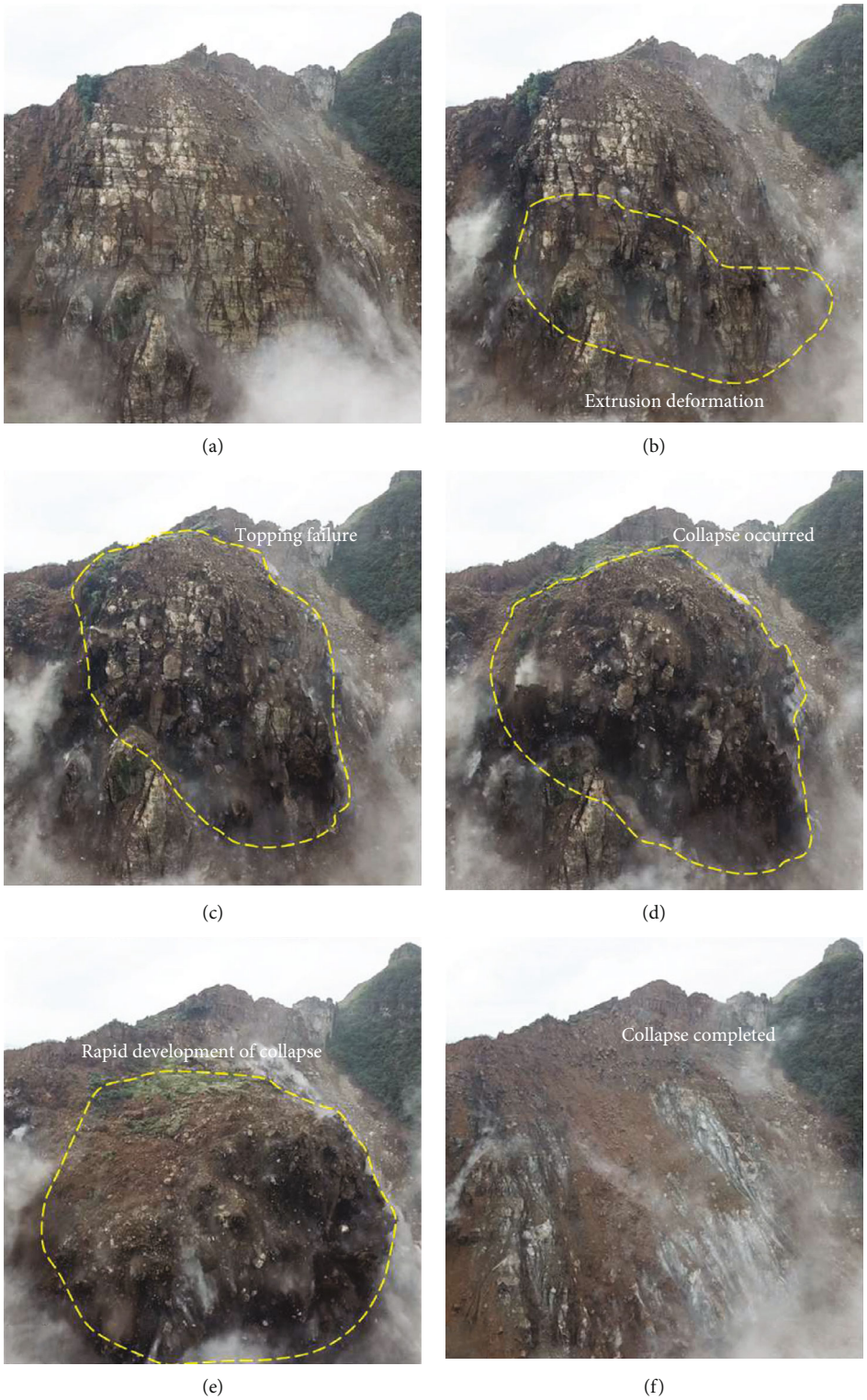

Figure 6: Eyewitness sample video frame for the progressive development of collapse.

4.1.1. Bottom Friction Test. The bottom friction model test simulates the gravitational force on the model by the friction between the model and the bottom surface. The basic principle is the model is flattened on the horizontal conveyor belt so that the original section depth direction is consistent with the direction of the conveyor belt movement (see Figure 7), the lower part of the model is blocked by the model frame, and the bottom of the model is blocked by frictional resistance at each point. The constraints of the structure are very similar to the two-dimensional geometric features of the ramp. The basic frictional force F is generated by the resistance caused by moving the belt, which is opposite to the

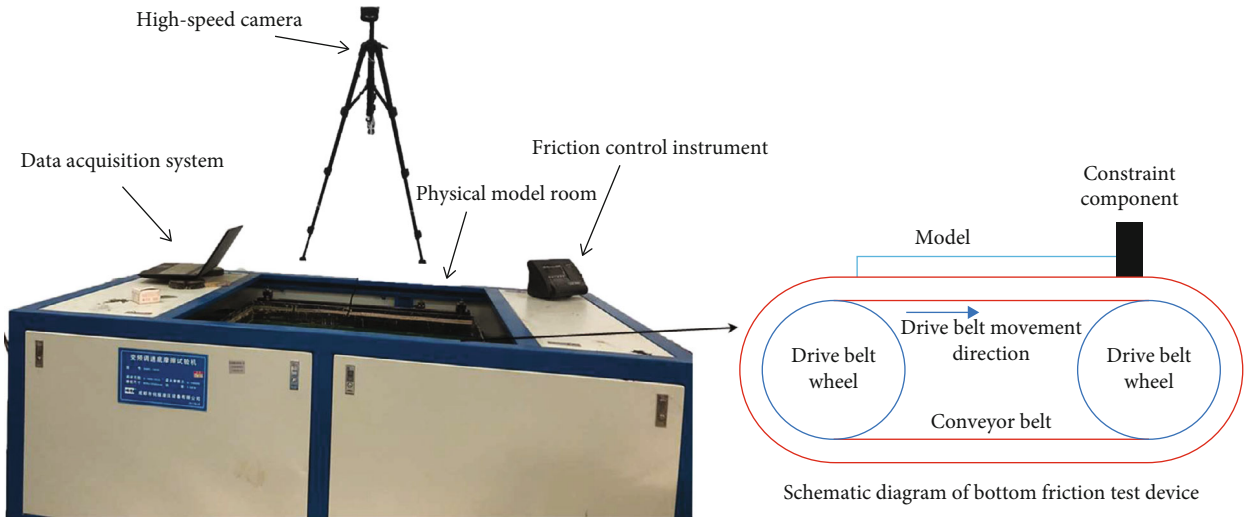

Figure 7: Bottom friction-based physical model test setup.

resistance generated by the fixed frame. The theory of base friction modeling can be expressed mathematically in the following equation:

$$F = \iint \gamma_m \mu d d z d w, \tag{1}$$

where γ_m is the unit weight of the material used in the model, d is the model's thickness, μ is the coefficient of friction between the model material and the belt, z is the length of the model, and ω is the width of the model.

According to The Saint-Venant principle, when the model is thin enough, friction can be considered to act evenly over the entire thickness, equivalent to the state in which the prototype object is subjected to gravity under natural conditions [41]. The physical model experiment is based on the principle of similarity, and a similar relationship between the research object and the model is established to ensure that the physical phenomena reflected in the model experiment are identical to the prototype [42]. The bottom friction test model is similar to the prototype and needs to meet certain similarities in terms of geometric conditions, force conditions, and friction coefficients [42].

4.1.2. PFC Numerical Simulation. PFC is a numerical method of disciple particle flow, which combines the contact model of the rigid disk with the contact model of the rigid sphere to form an equivalent rock model with appropriate strength. The mechanical characteristics of rock bodies are simulated through detailed strength and elastic parameters [43].

PFC can study the mechanical behavior of granular materials and simulate the rupture and separation of rocks and better simulate the rupture process and crack development process of rock masses. PFC is iterated in time steps, and each iteration is repeatedly applied to the laws of motion and the law of force-displacement. When the motion state of the mass is updated and the adjacent force between the outer force and the mass point changes, the system will automatically recalculate according to the theory of the force-displacement relationship. Contact forces and particle motion are updated until the system reaches a new equilibrium (see Figure 8). The law of particles follows Newton's second law of motion, which describes the rigid motion of individual particles by acting on the combined forces and force moment vectors acting on each particle. As a result, the rock mass model constructed by PFC can simulate the dynamic behavior of rock bodies in nature.

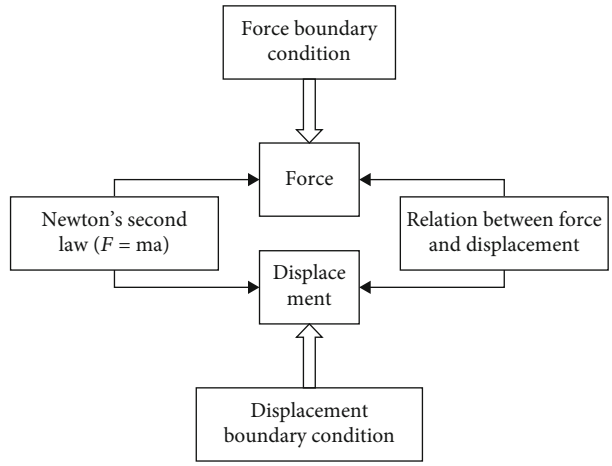

Figure 8: Process diagram of particle flow cycle calculation.

4.2. Theory. For rock slides that conform to a three-segment mechanism, they usually occur in slopes consisting of the following [44]: (a) brittle rocks or rocks with a nearly horizontal or gently inclined structural surface at the bottom of the slope; (b) hard rocks with a thin sandwich of weaker material. At the same time, coal seam excavation is also an important factor. Three-stage mechanism: sliding, tensile cracking, and shearing in sliding/tensile cracking/shearing mechanisms, deformation and failure processes can be described as

(1) During slope formation, unloading/rebound deformations are caused by postgenesis along the gentle structural surface at the bottom of the slope. After the coal seam is mined, the overlying rock mass is deformed. This results in tensile stress zones and tensile cracks at the top of the landslide, especially in high-stress zones (Figure 9)

(2) Subsequently, with the mining of multiple coal seams, the deformation intensifies. Under the long-term action of gravity, the slope is continuously crawling along the gentle structural surface, resulting in a deepening of the head crack (Figure 9)

(3) When the rear crack reaches a certain depth, the accumulated stress in the "locking section" causes the slope to break gradually. Finally, the "locking segment" will be destroyed by shear forces, and brittle damage will occur on the slope. Since such slopes often have considerable potential energy, the sliding velocity can be exceptionally high when disruption occurs

The field investigation results show that the morphology of the sliding surface of the general sprinkler is approximately circular, which is in line with this deformation and destruction mechanism. To verify this finding, the deformation failure mechanism of the general collapse and collapse of the general sprinkler was studied by using the physical simulation of the bottom friction test and the numerical simulation of the particle flow program (PFC). Since the "locking section" is essential for slope stability, the hazard protection strategy is to avoid damaging the section and take technical measures to inhibit the development of posterior cracks and/or increase the shear strength of the front of the slope.

5. Physical Simulation

5.1. Similarity Ratios and Physical Model. According to the similarity principle, the base friction model test was used to study the deformation and failure mechanism of Pusa collapse and reproduced the whole process of collapse deformation and failure. The model of the bottom friction test instrument is DMC-1000 variable frequency adjustable speed bottom friction test machine, and the template size of the variable frequency adjustable speed bottom friction test machine instrument is 800 mm × 1000 mm. The speed regulation range is 0 ~ 100 r/min. The friction force is 0 ~ 1000 N.

The main section of Pusa collapse was selected as the prototype for the experimental model. The upper part of the slope was mainly thin to medium thick limestone (T_1y^2), argillaceous siltstone (T_1y^1), and limestone (P_{3c+d}), and the lower part was mainly composed of mudstone and coal seam (P_3l). The lithologic structure was complex. Therefore, the model needs further generalization. T_1y^2 was generalized as limestone. T_1y^1 was generalized as limestone, P_{3c-d} was generalized as limestone, and P_3l was generalized into mudstone. According to the previous research results, combined with the actual original geological conditions, rock physical and mechanical parameters, and the size of test equipment, and after a series of reasonable trial simplifications, it was determined that the most feasible similarity ratio between the physical laboratory model and the real prototype was 1 : 800. The length and height of the physical laboratory model were chosen as 80 cm and 75 cm, respectively.

Consequently, the model size was designed to be 80 × 75 cm. Quartz sand, heavy crystal powder, liquid paraffin, and bentonite were adopted as similar materials, and a similar ratio in line with the actual situation of each rock stratum lithology was obtained. The physical and mechanical parameters of different types of rocks were set as the benchmark targets for determining the reasonable blending proportion of similar raw materials for each field stratum through carefully designed orthogonal tests. According to the results of the orthogonal tests, the blending ratio of similar raw materials resembling field limestone stratum was barite powder: quartz sand : paraffin = 59.5 : 31.5 : 9, the blending proportion of similar raw materials resembling field sandstone stratum was barite powder: quartz sand : paraffin = 65 : 25 : 10, the blending ratio of similar raw materials resembling field mudstone stratum was barite powder: quartz sand : bentonite : paraffin = 65 : 19 : 6 : 10, and the blending proportion of similar raw materials resembling field coal seam was barite powder: bentonite : paraffin = 80 : 11 : 9. The basic physical and mechanical parameters of similar materials were obtained by orthogonal tests and applied to the laboratory physical model test. The details were referred to elsewhere for brevity [45].

Coal seams are M16, M14, and M10. The dip angle was 7°, and a group of 85° structure planes in inclined slope was selected. The mining sequence of coal seam excavation was M16 → M14 → M10 from bottom to top. The M16 coal seam sets three mining areas and two coal pillars. M14 coal seam sets two mining areas and one coal pillar. M10 was located in the uppermost seam, and no coal pillar was left during mining. It had been mined twice, with the first mining depth of 10 cm and the second mining depth of 15 cm. To prevent the sudden damage of the physical laboratory model during mining, the reserved coal pillars were initially kept intact with a width of 4 cm. After the deformation tended to be approximately stable, the reserved coal pillars were then excavated to mimic typical field coal-mining operations in the study area. The schematic diagram of the physical laboratory model is shown in Figure 8, of which the structural layers were described previously in the field forensic investigation part. After the physical model was fabricated, it was let stand for 24 h. It was then placed onto the testing equipment to start the physical model test.

5.2. Physical Simulation Results. Based on the results of the experiment, the evolution process of the experimental model can be divided into four stages.

5.2.1. Deformation Stage of Overburden. After the M16 coal seam was completed, the overlying rock mass slightly bent and subsided under gravity, and slight cracks appeared near the roof. With the excavation of the M14 coal seam, the roof of the coal seam was further deformed, and cracks grew and widened gradually.

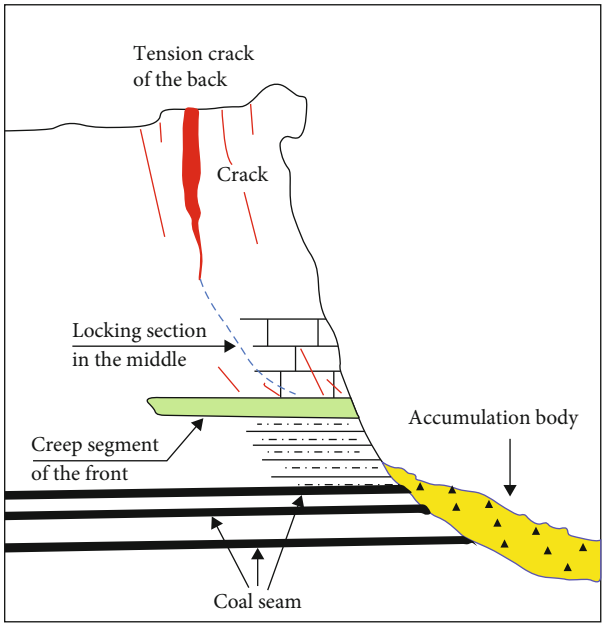

Figure 9: The three-section mechanism of a landslide [40].

The M10 coal seams were excavated twice. After the first 10 cm, the coal seam was mined, the roof of the coal seam subsided, and there was a separation between the layers. The separation interval was about 1 mm. The joints on the top of the slope showed signs of being pulled apart and developing downward, and crack LF2 was gradually formed, as shown in Figure 10(a).

5.2.2. The Formation Stage of the Top Crack in Slope and Goaf Collapse. After the M10 coal seam and coal pillar of the M14 coal seam were mined, the roof of the coal seam bent and sunk to the goaf, and the overlying rock of the goaf formed a fracture zone and collapsed downward. With the continuous expansion of the collapse area, the upper rock mass bent downward and sunk layer by layer, which caused the collapsed arch to become larger and the cracks on the top of the slope to become wider. The tension cracks near the goaf continue to extend to the top of the slope. The main fracture of LF1 at the rear edge has been opened about 8 mm, and the lower crack also shows a trend of connecting. The rock mass in front of the slope opened along the primary structural plane and developed downward to form fracture LF2, as shown in Figure 10(b).

5.2.3. Stage of Crack Through and Slip Surface Formation. The main crack LF1 was gradually widened, the width was increased from the original 8 mm to 12 mm, and it ran down to the goaf to cut the rock bridge. The upper rock mass lost its support, the whole rock mass staggered downward, and the downward displacement was about 5 mm. Due to the influence of the free face of the front edge of the slope and the concave rock cavity in the lower part of the olecranon, the crack LF2 gradually widened, and the vertical structure of the track developed downward, with a width of about 2 mm. When the instrument ran for a while, the front edge of the slope toppled forward, and the gravity center of the rock mass deflected. The cracks develop downward. Meanwhile, they were affected by the gravity deflection. When the cracks develop to the soft rock of the second member of Yelang formation in the lower part, the cracks no longer developed downward due to the low strength of the soft rock but cut out to the slope under the self-weight of the upper rock mass and shear the lower rock mass, as shown in Figure 10(c).

5.2.4. Failure Stage of Slope Instability. With the expansion of the influence scope of the collapse area, the cracks became wider and longer, and the rock mass became more damaged, which further aggravated the collapse failure of the rock mass to the free face. When the rock mass was constantly toppling towards the free face, the LF2 crack was pulled apart, and the distance between them became larger. Under gravity, LF2 fracture expanded downward, and rock mass collapse occurred. In the process of downward rolling, the avalanches collided with each other, disintegrated gradually, and accumulated in the front edge of the slope surface. The main fracture LF1 is pulled to 2.5 cm (Figure 10(d)).

Due to coal mining, the overburden is disturbed, resulting in the adjustment of internal stress. The slope has sequentially experienced the process of coal seam roof collapse, expansion deformation, tensile cracking, and slope collapse. After the coal seam roof collapses, an arch-shaped collapse area is formed. With the goaf's expansion, the goaf's collapse area is also expanding, and the collapse deformation is transmitted to the slope top, creating cracks on the slope top. The tensile fracture at the top of the slope no longer extends downward but extends to the soft rock with low strength, the "locking section" of the cutting front, and the upper rock mass is unstable. Finally, after the deformation exceeds the stability limit, the slope collapses, and the collapse debris then stays and accumulates at the broken foot of the physical model. The front rock mass is unstable and collapses, and some remaining collapses from cliffs. Since there is no barrier at the front edge, dangerous rock mass may collapse under natural conditions. These results are consistent with the results of field forensic investigation, which can truly reflect the slope deformation and failure process and can further confirm the rationality of the subsequent numerical simulation results.

6. Numerical Simulation

6.1. Rock Parameters. In this paper, the mechanism of slope deformation induced by picking in Nagao County is analyzed numerically by the PFC method. DEM can better simulate the micromechanical response of rock mass; however, the micromechanical parameters required as PFC input are usually not directly related to the macro strength parameters. Before using PFC, it is necessary to calibrate its parameters. Parameter calibration means that the detailed parameters of the discrete unit must match the macrorock parameters. To obtain reliable parameters of rock mass, a series of tests such as the uniaxial compression test and direct shear test were carried out on the standard specimens of limestone and mudrock. The results are shown in Table 1.

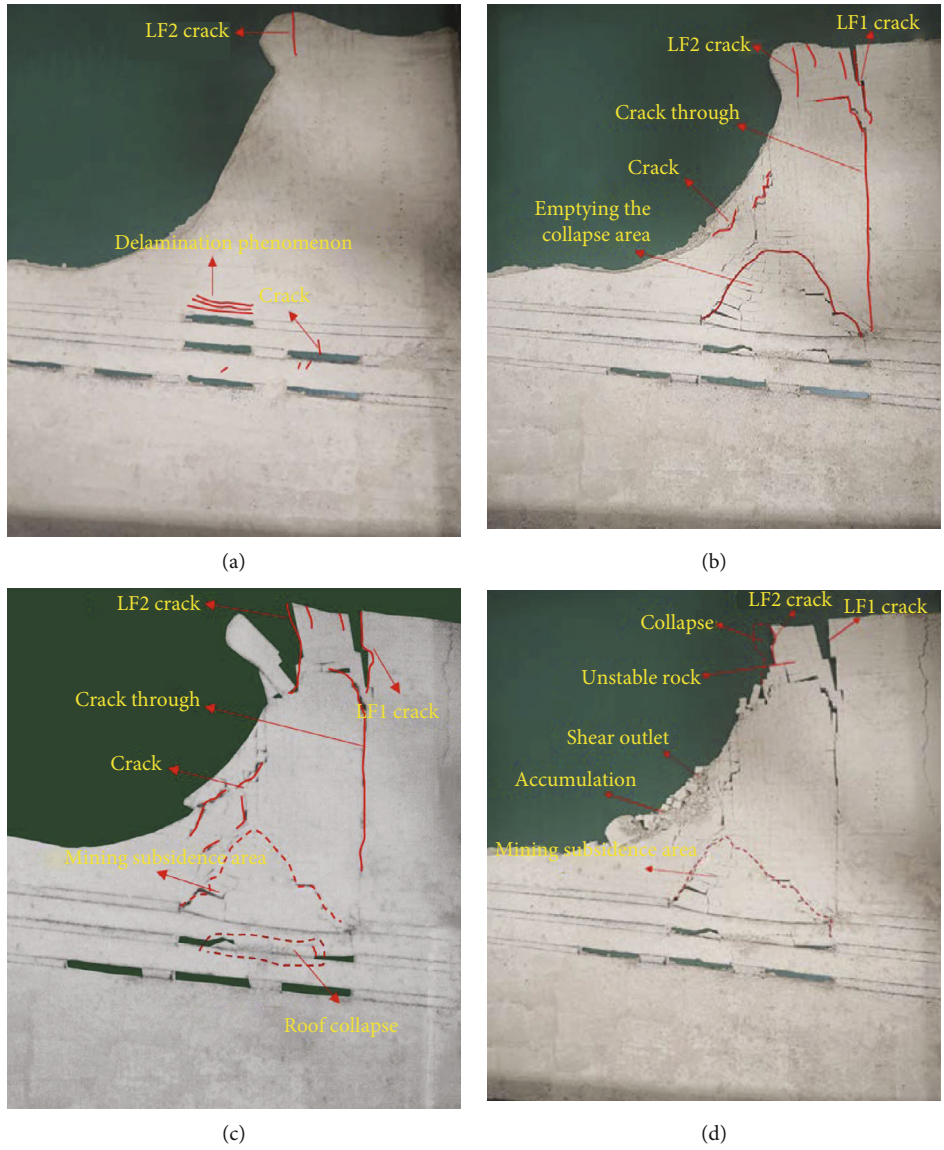

Figure 10: Process of deformation before the toppling failure. (a) The deformation feature of the cladding rock. (b) Deformation of mined-out areas and cracks on the top of the slope. (c) Dumping damage feature map. (d) Slope failure after instability.

Table 1: Macroparameter values for limestone and fracture plane.

Parameter	σ_c (MPa)	E_c (MPa)	ν	C (MPa)	φ (°)
1#	74.5	19.1	0.23	0.45	39
2#	75.9	22.6	0.18		
3#	74.9	18.9	0.16		
Average value	75.10	20.20	0.19		

σ_c is uniaxial compressive strength; E_c is the modulus of elasticity; ν is Poisson's ratio; C is the cohesion of the fracture plane; φ is the friction angle of the fracture plane.

Please note that the physical and mechanical parameters are comprehensive laboratory databases developed by the authors and other team members [45–48]. It may not be appropriate to directly apply the features obtained from laboratory tests to the PFC model. According to the parameters obtained from the tests, the parameters are calibrated using a parallel bonding model and smooth technology model to simulate the mechanics of rocks.

According to the size of the simulation model and the calculation efficiency of the computer, it is comprehensively determined that the particle size is 0.3-0.49 m, the porosity is 12%, the model sample is 50 m × 100 m, and the number of sample particles generated is 8846. Since the simulation test is a reproduction of the indoor test, the purpose is to reflect the macroparameters into the microparameters and then calibrate the macroparameters through the simulation test with the microparameters. The uniaxial compression test is also designed in the model test to obtain the stress-strain curves of limestone and mudstone (Figure 11), and then, the microscopic parameters of limestone and mudstone are calculated. The results of parameter calibration are shown in Table 2.

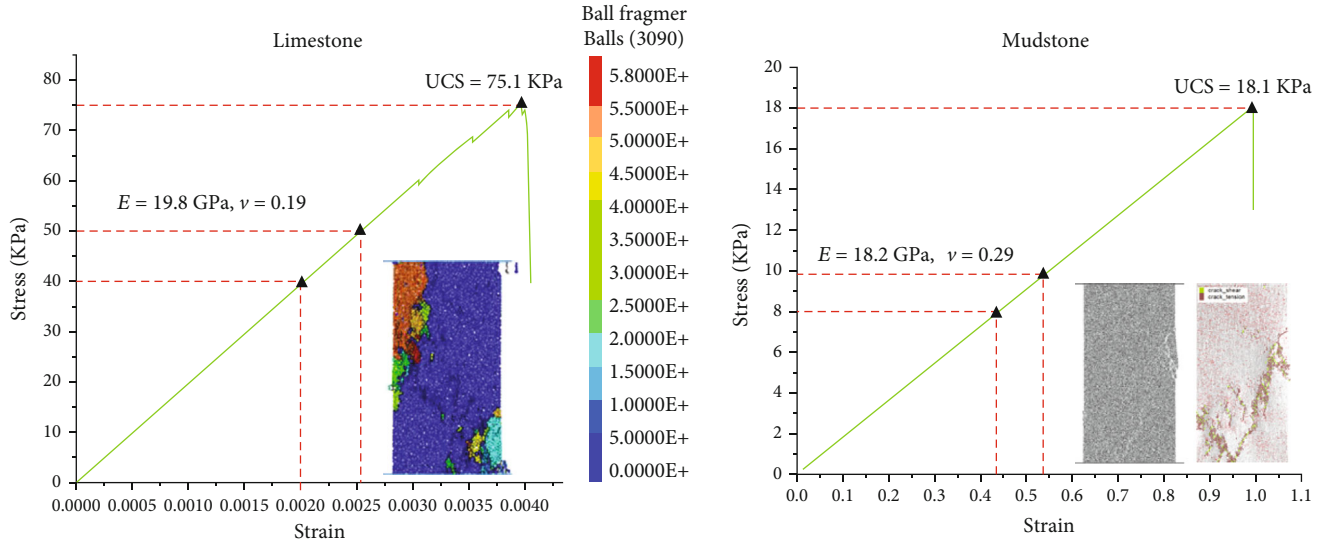

Figure 11: Calibration curve of limestone and mudstone parameters.

Table 2: Rock and fracture plane microstrength parameters.

Parameters	Limestone	Mudstone
Model height (m)	100	—
Model width (m)	50	—
Particle size (m)	0.3-0.49	—
Porosity (%)	12	—
Particle density (kg/m^3)	2700	2620
Particle friction coefficient (μ)	0.8	0.51
Bond radius ratio (λ)	0.2	0.2
Elastic modulus of linear (GPa)	20	6
Linear stiffness ratio (kn/ks)	2.2	2.4
Elastic modulus of parallel bond (GPa)	19	5.1
Parallel bond stiffness ratio ($(\overline{k\_n})/(\overline{k\_s})$)	2.2	2.4
Tensile strength (MPa)	11.1	7
Cohesion (MPa)	10	6

6.2. Numerical Model. The deformation process of the Pusa slope was simulated using the PFC 2D model. The results were further analyzed to verify the failure mechanism. Based on the terrain before the collapse and the nearby landform, this paper reconstructs the two-dimensional discrete element model based on the best main section of the slope. The model, 350 m in height and 800 m in length, consisted of 50,000 particles. Figure 12 shows a numerical model constructed based on the longitudinal section in Figure 2(c). Several straight lines were used to build the slope surface in the model. To better reflect the deformation and failure process of the slope, the geological conditions were simplified. For example, the faults were not considered, and the rock mass only has four types: limestone layer, argillaceous limestone layer, sandy mudstone layer, and coal layer. The coal seam was composed of strata represented by M16, M14, and M10. In this study, PFC built-in model was adopted for the numerical model with required physical

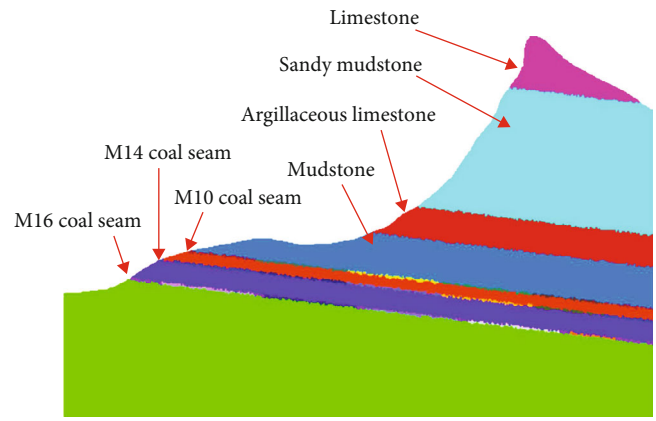

Figure 12: Schematic profile of numerical model.

and mechanical input parameters is shown in Table 2. The geometrical characteristics of joints were simulated, referring to the study reported by Zhao et al. [12]. Considering most of the joint interfaces were relatively smooth, and the gaps were not in-filled, it is assumed that the bond strength and joint friction coefficient are negligible. The lateral and bottom boundaries of the model were fixed, and a stress/strain-controlled deformation was applied. The stress field of the model only considers the gravity field, and the tectonic stress was not considered in the analysis.

6.3. Numerical Simulation Results. Based on field data, numerical simulations, and a previous study [13], the destruction process of the collapse can be summarized in four stages [49], as shown in Figure 13.

6.3.1. Deformation Stage of Goaf Roof. Due to underground mining activity, the overlying rock mass in the goaf was disturbed, destroying the initial balance state inside the slope. As the overburdened rock of the goaf roof was deformed by the mining stress field and gravitational stress field, the

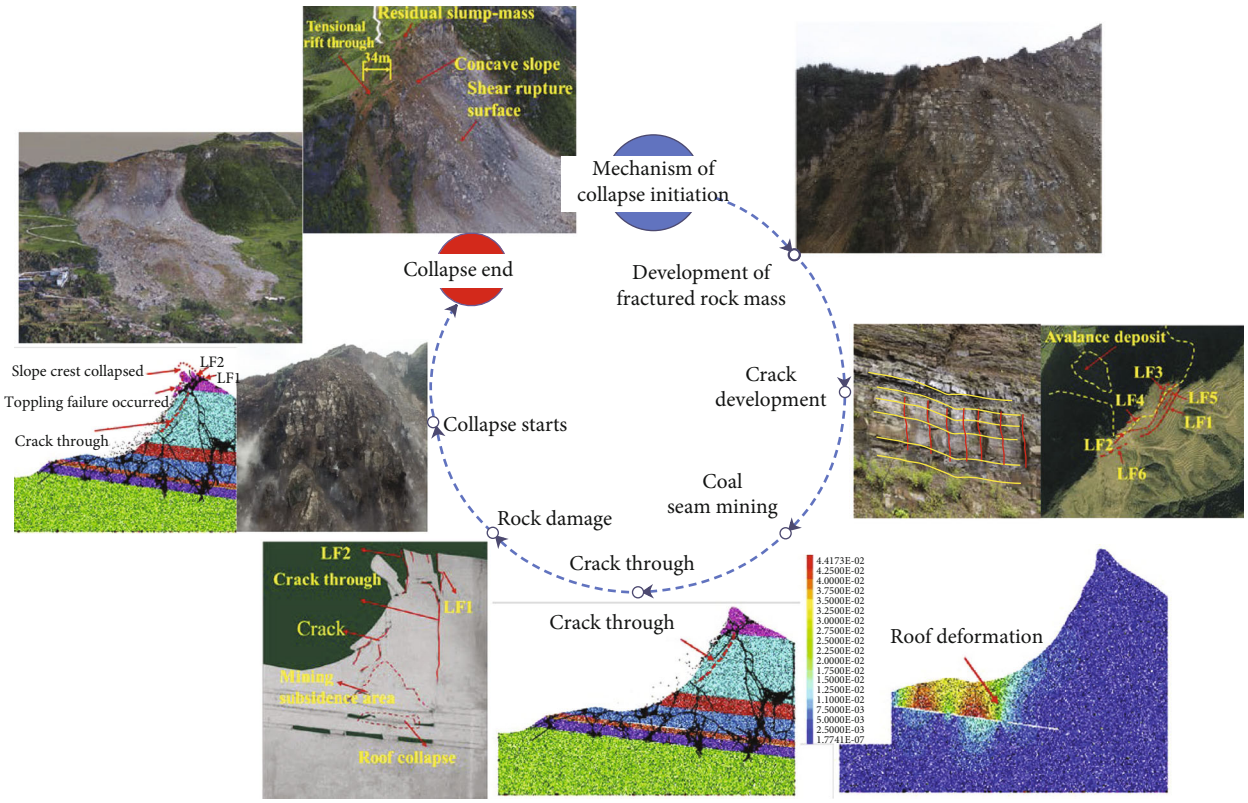

Figure 13: The model-predicted initiation and evolution process of the slope collapse.

roof began to crack apart, as shown in Figure 14(a). Then, the overlying rock mass on the goaf boundary deformed outwards and eventually developed deep tension cracks.

6.3.2. Formation Stage of Slope Top Crack. After a period of mining of M10 and M16 coal seams, the loss of support for the roof of goaf led to increased deformation and gradual destruction of overburden. At the same time, with the balance state being damaged near the goaf, the stress concentration area occurred, the cracks were produced and gradually developed upward, and the overburdened rock of the goaf formed fracture zone as shown in Figure 14(b). Then, the roof of the goaf also began to bend and sink. As mining activities continued, the roof of the goaf further subsided, deformed, and collapse, forming a caving zone and rapidly extended upward along the steep joint surface. With the development of deformation, cracks propagated to the crest of the slope, as shown in Figure 14(c).

6.3.3. Intensification Stage of Deformation. As the M10 coal seam mining process developed, the goaf further collapsed, which made rock mass lose and weakened the stability of rock mass. Under gravity, stress concentration would arise at the top of the slope and slope table, and the tensile cracks at the back edge extended downward to form deep cracks. After mining was stopped for several years, the retained coal pillars between the goaves could not withstand the upper pressure, which aggravated the deformation of overburdened rock in goaf. Thus, the cracks expanded upward, and the rock bodies became more damaged. Meanwhile, the original cracks in the top of the slope increased, and the fissures above the mining area extended to the top of the slope, as shown in Figure 14(d). With the development of cracks, cracks also appeared in the middle of the slope. The top of the slope crack was also expanding downwards, gradually with the middle cracks, forming a potential slip surface. Due to the influence of the surface, the mining area, and the rainfall, the top rock mass of the slope began to decline.

6.3.4. Stage of Collapse. With the continuous upward development of the impact range of the collapse, more cracks emerged, and the whole slope produced an uneven settlement, resulting in a large number of cracks in the top of the slope. The increase in cracks led to a significant fragment of the rock, and dumping damage begins at the top of the slope, as shown in Figure 14(e). Tensile cracks in the upper hard rock formation form potential sliding surfaces by connecting. Under the pressure of the upper hard rock layer, the shear damage in the middle of the slope was formed in the soft and hard mutual layer, as shown in Figure 14(f). Under the external forces, the final collapse occurred, and the collapse was affected by the impact-shovel scraping, moving at high speed in the form of debris flow, piling up at the foot of the slope.

6.4. Discussion on Failure Mechanism of Pusa Collapse. Comparing Figures 11 and 14, it could be concluded that

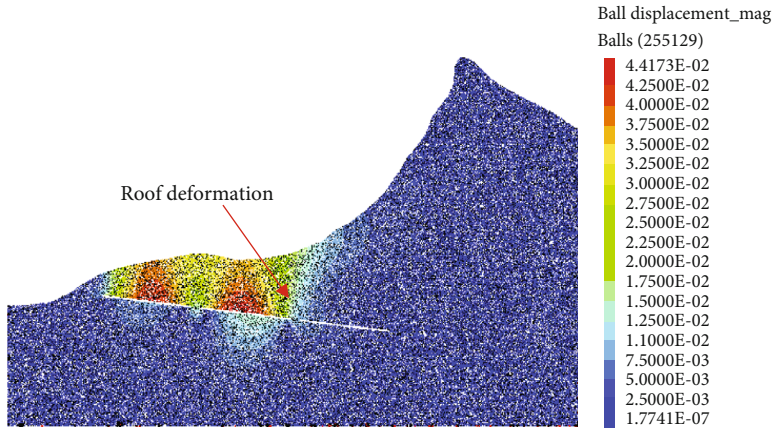

(a)

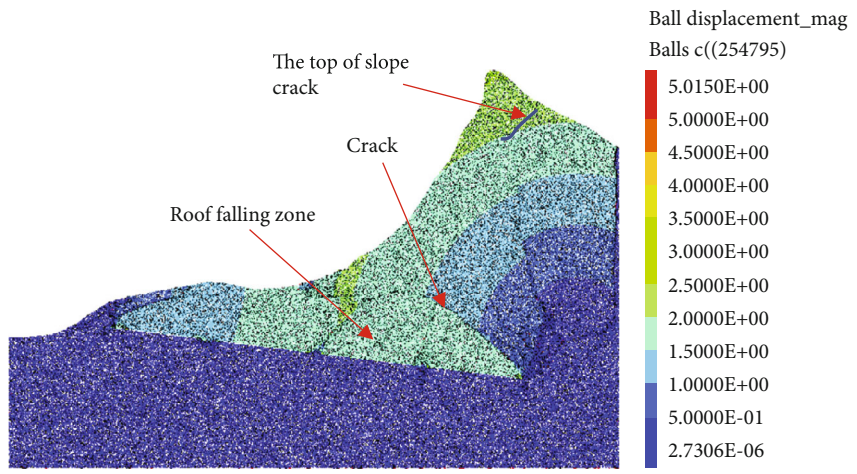

(b)

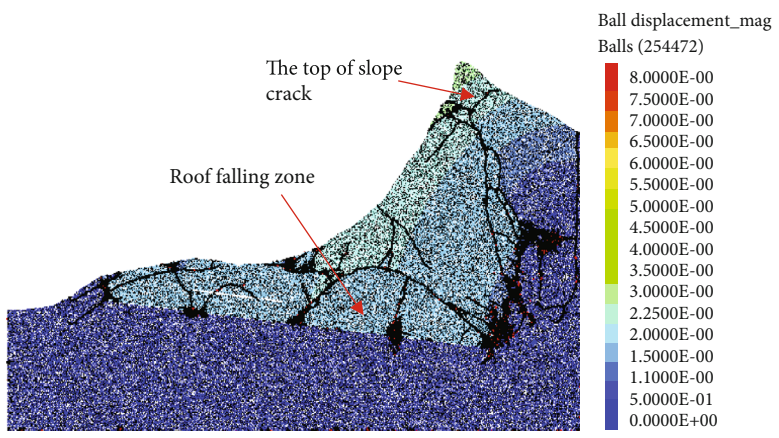

(c)

Figure 14: Continued.

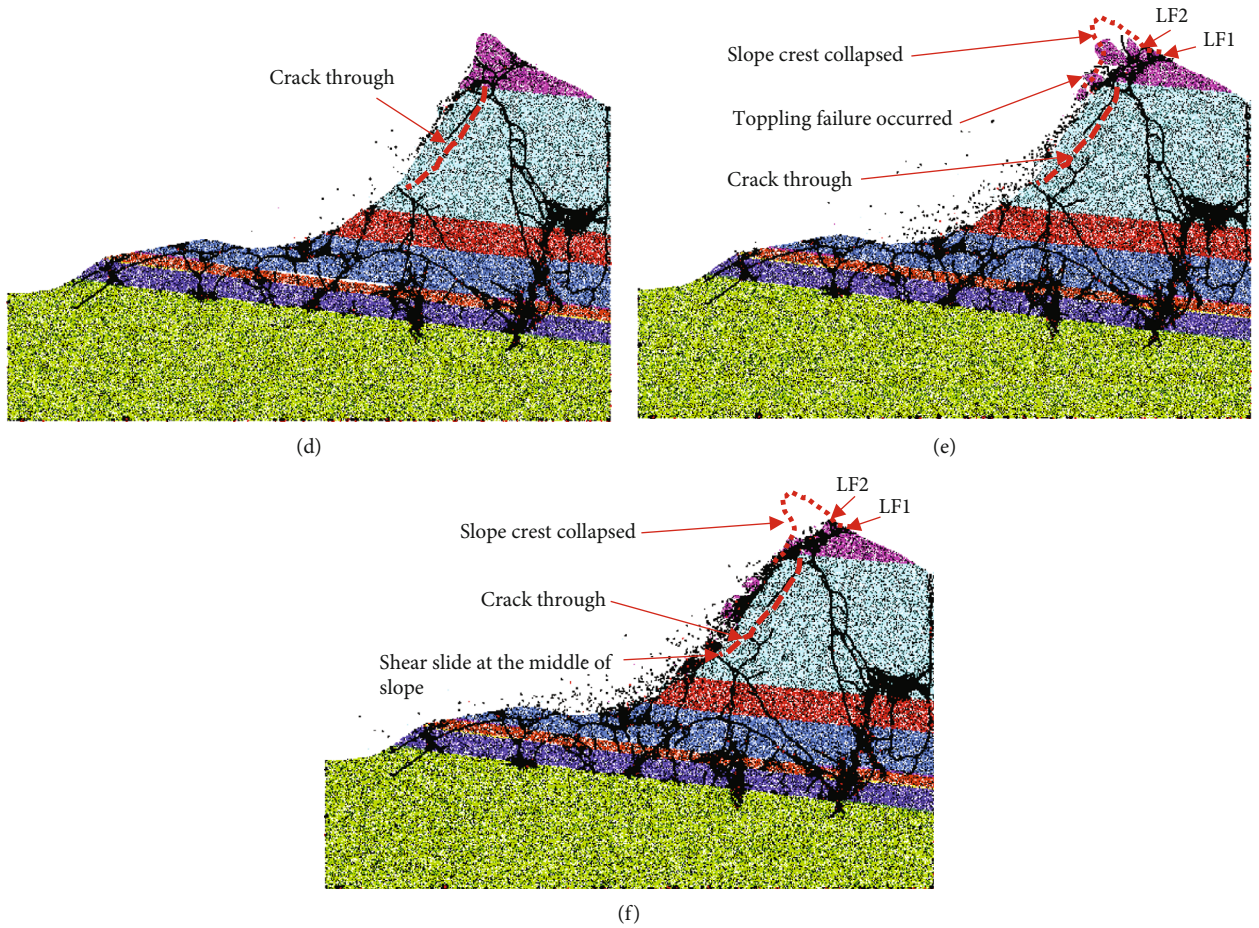

Figure 14: Failure process of the Pusa collapse.

the results of the base friction test are in good agreement with the numerical simulation. After the analysis of the base friction test and numerical simulation, the failure mechanism of Pusa collapse was discussed in this section.

The occurrence of the collapse studied is caused by both internal and external factors. There are unique geological and stratigraphic structures in this area, and two groups of nearly vertical fractures have already existed within the slope. Such fractures cut the intact rock masses into discontinuous blocks and provide channels for infiltrated precipitation; thus, the rock masses of the slope are relatively fractured and disintegrated, which provides indispensable physical conditions triggering the development of the collapse (Figure 13).

The upper slope was composed of high-strength limestone, and the formation of the toppling failure mainly depended on the mining intensity, high steep terrain, and geological conditions. After the coal seam is excavated, the fractured rock masses in the slope are susceptible to deformation disturbance. With the goaf's expansion, the goaf's roof sinks, the cracks expand upward along the joint direction, and cracks appear on the top of the slope. In addition, with the further mining of the coal seam, part of the fracture surfaces starts debonding. The tensile stress within the overlying rock masses is transmitted to the back edge of the slope and becomes connected, resulting in the tensile deformation of the back edge of the slope. After the coal seams are excavated, the cracks on the top of the slope gradually expand, and rock masses become more broken, resulting in the loss of strength, which makes rock mass bend forward and in turn and then toppling failure occurs.

A soft rock exists in the middle of the slope. With the continuous advancement of coal mining, the scope of goaf becomes larger, and the roof of goaf begins to fall, forming cracks near the coal pillar and overburden rock. The cracks mainly extend upward along the direction of the joint and form cracks in the middle of the slope. Due to the emergence of more tensile cracks, the whole mountain mass is deformed towards the free face under gravity. When the deformation value exceeds the critical value of equilibrium, the middle and lower parts of the slope are damaged. While cracks in the middle of a slope are connected to cracks in the upper slope; thus, a shear–sliding failure is formed. Then, the whole upper rock masses fall, scrape, and move forward together with the lower part of rock masses. This model-predicted initiation and evolution of the slope collapse process agree well with the field observation.

Therefore, the mechanism of destruction of the collapse is summarized as 1. Goaf subsides,crack toppling failure in the upper slope and shear-sliding failure in the middle of the slope.

7. Conclusion

Pusa collapse is a typical example of the deformation and failure of the antidip slope. Mining activities aggravate the deformation of the overlying rock mass, which makes the cracks further expand and leads to the instability of the upper slope. The failure factors of landslides are closely related to the unique geological conditions of slopes, underground mining activities, and topography. Underground mining is the decisive factor inducing landslides.

Based on the field investigation results, this paper analyses the destruction process and mechanism of Pusa collapse using the base friction test and PFC2D numerical simulation. The results of the base friction test show that the destruction process of the collapse includes the rock deformation stage, slope top formation stage, mining collapse formation stage, the crack through and slip surface formation stage, and slope instability failure stage. The numerical simulation results show that the collapse destruction process includes the stage of the deformation and development stage of the roof of the mining area, the stage of the development stage of the top crack of the slope, the aggravation of the deformation, and the occurrence of collapse.

The results of the base friction test are consistent with the numerical simulation. The destruction of collapse can be summarized as the stage of deformation and development of the top plate of the mining area, the stage of the development stage of the top crack of the slope, the worsening of deformation, and the stage of crack passage and collapse. The presence of weak rock formations and upper hard rock formations in the middle creates favorable conditions for cracks. The high-strength rock stratum developed on the slope has cracking-toppling failure; At the same time, the slope on the low-strength rock stratum also has collapse-rip-slip failure. The collapse destruction mechanism results from joint action of crack-dumping damage and collapse-pull-slip destruction. Therefore, the collapse mechanism is summarized as collapse-pull-dump-slip destruction, accompanied by a large number of collapses piled up at the foot of the slope.

The results of field investigation and physical model tests indicated that the instability of the slope was initiated from the middle and lower parts. The failure of rock masses in such areas weakened the support and triggered the collapse of the upper area of the mountain mass.

The safety and development of the mining area require improvement in the mining methods and understanding the mechanism of collapse and destruction. Collapse occurs when a crack is formed at the top of the slope and near the middle of the slope. Therefore, the formation of cracks in different parts of the slope can be observed in this study, which is an early identification factor marker for large-scale mining collapse.

Data Availability

Data is available upon request.

Conflicts of Interest

The authors declare no conflicts of interest.

Authors' Contributions

The first author is Shaozhen Xiong.

Acknowledgments

This study is financially supported by the National Natural Science Foundation of China (Grant no. 42067046) ,Science and Technology Planning Project of Guizhou Provincial, China (Grant no. QKHJC-ZK[2021]YB228), and Science and Technology Projects of Guizhou Provincial, China (Grant no. QKHJC-ZK[2022] YB075).

References

[1] Y. P. Yin, P. Sun, M. Zhang, and B. Li, "Mechanism on apparent dip sliding of oblique inclined bedding rockslide at Jiweishan, Chongqing, China," *Landslides*, vol. 8, no. 1, pp. 49–65, 2011.

[2] S. M. Moreiras, "Climatic effect of ENSO associated with landslide occurrence in the Central Andes, Mendoza Province, Argentina," *Landslides*, vol. 2, no. 1, pp. 53–59, 2005.

[3] M. J. Froude and D. N. Petley, "Global fatal landslide occurrence from 2004 to 2016," *Natural Hazards and Earth System Sciences*, vol. 18, no. 8, pp. 2161–2181, 2018.

[4] R. Q. Huang, "Large-scale landslides and their sliding mechanisms in China since the 20th century," *Chinese Journal of Rock Mechanics and Engineering*, vol. 26, no. 3, pp. 433–454, 2007.

[5] G. J. McCall, *Geohazards: Natural and Man-Made*, Springer Science & Business Media, 2012.

[6] G. Y. Zhao, B. Dai, and C. Ma, "Study of effects of microparameters on macroproperties for parallel bonded model," *Chinese Journal of Rock Mechanics and Engineering*, vol. 31, no. 7, pp. 1491–1498, 2012.

[7] R. Q. Huang, Q. Xu, and J. Huo, "Mechanism and geomechanics models of landslides triggered by 5.12 Wenchuan earthquake," *Journal of Mountain Science*, vol. 8, no. 2, pp. 200–210, 2011.

[8] Q. Xu, X. M. Fan, and X. Dong, "Characteristics and formation mechanism of a catastrophic rainfall–induced rock avalanche–mud flow in Sichuan, China, 2010," *Landslides*, vol. 9, no. 1, pp. 143–154, 2012.

[9] Q. Wu and P. H. S. W. Kulatilake, "REV and its properties on fracture system and mechanical properties, and an orthotropic constitutive model for a jointed rock mass in a dam site in China," *Computers and Geotechnics*, vol. 43, pp. 124–142, 2012.

[10] Y. Y. Jiao, Z. H. Wang, X. Z. Wang, A. C. Adoko, and Z. X. Yang, "Stability assessment of an ancient landslide crossed by two coal mine tunnels," *Engineering Geology*, vol. 159, pp. 36–44, 2013.

[11] P. H. S. W. Kulatilake and Y. F. Ge, "Investigation of stability of the critical rock blocks that initiated the Jiweishan landslide in China," *Geotechnical and Geological Engineering*, vol. 32, no. 5, pp. 1291–1315, 2014.

[12] J. J. Zhao, J. G. Xiao, M. L. Lee, and Y. T. Ma, "Discrete element modeling of a mining-induced rock slide," *Springerplus*, vol. 5, no. 1, p. 1633, 2016.

[13] X. M. Fan, Q. Xu, G. Scaringi et al., "The "long" runout rock avalanche in Pusa, China, on August 28, 2017: a preliminary report," *Landslides*, vol. 16, no. 1, pp. 139–154, 2019.

[14] Y. Q. Zhu, S. M. Xu, Y. Zhuang, X. Dai, G. Lv, and A. Xing, "Characteristics and runout behaviour of the disastrous 28 August 2017 rock avalanche in Nayong, Guizhou, China," *Engineering Geology*, vol. 259, p. 105154, 2019.

[15] T. Sherizadeh and P. H. S. W. Kulatilake, "Assessment of roof stability in a room and pillar coal mine in the U.S. using three-dimensional distinct element method," *Tunnelling and Underground Space Technology incorporating Trenchless Technology Research*, vol. 59, pp. 24–37, 2016.

[16] X. Li, S. J. Wang, T. Y. Liu, and F. S. Ma, "Engineering geology, ground surface movement and fissures induced by underground mining in the Jinchuan nickel mine," *Engineering Geology*, vol. 76, no. 1-2, pp. 93–107, 2004.

[17] F. Q. Tang, "Research on mechanism of mountain landslide due to underground mining," *Journal of Coal Science and Engineering*, vol. 15, no. 4, pp. 351–354, 2009.

[18] Y. Hu, F. Ren, H. Ding, Y. Fu, and B. Tan, "Study on the process and mechanism of slope failure induced by mining under open pit slope: a case study from Yanqianshan iron mine, China," *Advances in Civil Engineering*, vol. 2019, Article ID 6862936, 26 pages, 2019.

[19] M. Marschalko, I. Yilmaz, M. Bednárik, and K. Kubečka, "Deformation of slopes as a cause of underground mining activities: three case studies from Ostrava–Karviná coal field (Czech Republic)," *Environmental Monitoring and Assessment*, vol. 184, no. 11, pp. 6709–6733, 2012.

[20] C. L. Tang, J. C. Hu, M. L. Lin et al., "The Tsaoling landslide triggered by the chi-chi earthquake, Taiwan: insights from a discrete element simulation," *Engineering Geology*, vol. 106, no. 1-2, pp. 1–19, 2009.

[21] W. Li, S. Mei, S. Zai, S. Zhao, and X. Liang, "Fuzzy models for analysis of rock mass displacements due to underground mining in mountainous areas," *International Journal of Rock Mechanics and Mining Sciences*, vol. 43, no. 4, pp. 503–511, 2006.

[22] X. Li, Q. Li, Y. Hu et al., "Study on three-dimensional dynamic stability of open-pit high slope under blasting vibration," *Lithosphere*, vol. 2021, no. 6426550, pp. 1–17, 2022.

[23] Z. Dou, Y. Liu, X. Zhang et al., "Influence of layer transition zone on rainfall-induced instability of multilayered slope," *Lithosphere*, vol. 2277284, p. 2021, 2021.

[24] B. H. Brady and E. T. Brown, *Rock Mechanics: For Underground Mining*, Springer Science & Business Media, 2013.

[25] O. Hungr, S. G. Evans, M. J. Bovis, and J. N. Hutchinson, "A review of the classification of landslides of the flow type," *Environmental and Engineering Geoscience*, vol. 7, no. 3, pp. 221–238, 2001.

[26] Y. H. Song, D. X. Nie, and C. H. E. N. Long, "Analysis on deformation and failure model of excavating slope and prediction," *Journal of Calamity*, vol. 18, no. 2, pp. 32–37, 2003.

[27] Z. Yang, Y. Jiang, B. Li, Y. Gao, X. Liu, and Y. Zhao, "Study on the mechanism of deep and large fracture propagation and transfixion in karst slope under the action of mining," *Journal of Geomechanics*, vol. 26, no. 4, pp. 459–470, 2020.

[28] F. P. Cui, B. Li, C. Xiong et al., "Dynamic triggering mechanism of the Pusa mining-induced landslide in Nayong County, Guizhou Province, China," *Geomatics, Natural Hazards and Risk*, vol. 13, no. 1, pp. 123–147, 2022.

[29] G. B. Crosta, S. Imposimato, and D. G. Roddeman, "Numerical modelling of large landslides stability and runout," *Natural Hazards and Earth System Sciences*, vol. 3, no. 6, pp. 523–538, 2003.

[30] M. Barla, G. Piovano, and G. Grasselli, "Rock slide simulation with the combined finite-discrete element method," *International Journal of Geomechanics*, vol. 12, no. 6, pp. 711–721, 2012.

[31] Y. G. Zhang, Z. Zhang, S. Xue, R. Wang, and M. Xiao, "Stability analysis of a typical landslide mass in the Three Gorges Reservoir under varying reservoir water levels," *Environmental Earth Sciences*, vol. 79, no. 1, pp. 243–254, 2020.

[32] D. Zheng, J. D. Frost, R. Q. Huang, and F. Z. Liu, "Failure process and modes of rockfall induced by underground mining: a case study of Kaiyang Phosphorite mine rockfalls," *Engineering Geology*, vol. 197, pp. 145–157, 2015.

[33] E. Eberhardt, D. Stead, and J. Coggan, "Numerical analysis of initiation and progressive failure in natural rock slopes–the 1991 Randa rockslide," *International Journal of Rock Mechanics and Mining Sciences*, vol. 41, no. 1, pp. 69–87, 2004.

[34] Y. G. Zhang, J. Tang, Z. Y. He, J. Tan, and C. Li, "A novel displacement prediction method using gated recurrent unit model with time series analysis in the Erdaohe landslide," *Natural Hazards*, vol. 105, no. 1, pp. 783–813, 2021.

[35] H. Q. Yang, Y. F. Lan, L. Lu, and X. P. Zhou, "A quasi-three-dimensional spring-deformable-block model for runout analysis of rapid landslide motion," *Engineering Geology*, vol. 185, pp. 20–32, 2015.

[36] L. Jing and J. A. Hudson, "Numerical methods in rock mechanics," *International Journal of Rock Mechanics and Mining Sciences*, vol. 39, no. 4, pp. 409–427, 2002.

[37] D. M. Cruden and C. D. Martin, "Before the frank slide," *Canadian Geotechnical Journal*, vol. 44, no. 7, pp. 765–780, 2007.

[38] M. Marschalko, I. Yilmaz, M. Bednárik, and K. Kubečka, "Influence of underground mining activities on the slope deformation genesis: Doubrava Vrchovec, Doubrava Ujala and Staric case studies from Czech Republic," *Engineering Geology*, vol. 147-148, pp. 37–51, 2012.

[39] C. Carnec and C. Delacourt, "Three years of mining subsidence monitored by SAR interferometry, near Gardanne, France," *Journal of Applied Geophysics*, vol. 43, no. 1, pp. 43–54, 2000.

[40] B. Benko and D. Stead, "The frank slide: a reexamination of the failure mechanism," *Canadian Geotechnical Journal*, vol. 35, no. 2, pp. 299–311, 1998.

[41] X. Chen, Y. Li, and X. Zhao, "The application of base friction test in the study of stability of rock mass toppling," *Earth Science Frontiers*, vol. 5, pp. 300–304, 2008.

[42] G. J. Cai, R. Q. Huang, and M. Yan, "Physical simulation study on deformation and failure response of an anti-inclined slope during excavation," *Chinese Journal of Rock Mechanics and Engineering*, vol. 27, no. 4, pp. 811–817, 2008.

[43] D. O. Potyondy and P. A. Cundall, "A bonded-particle model for rock," *International Journal of Rock Mechanics and Mining Sciences*, vol. 41, no. 8, pp. 1329–1364, 2004.

[44] R. Q. Huang, "Mechanisms of large-scale landslides in China," *Bulletin of Engineering Geology and the Environment*, vol. 71, no. 1, pp. 161–170, 2012.

[45] X. X. Yu, *Study on Deformation and Failure Mechanism of Gentle Anti Dip Mining Slope in Karst Mountainous Area*, Guizhou University, 2020.

[46] W. Xiaoming, X. Yuanjie, S. Wenbing, R. Juanjuan, C. Zhengxing, and L. Hua, "Research on meso-scale deformation and failure mechanism of fractured rock mass subject to biaxial compression," *Arabian Journal of Geosciences*, vol. 14, no. 14, 2021.

[47] X. M. Wang, Y. J. Xiao, W. B. Shi et al., "Forensic analysis and numerical simulation of a catastrophic landslide of dissolved and fractured rock slope subject to underground mining," *Landslides*, vol. 19, no. 5, pp. 1045–1067, 2022.

[48] S. Z. Xiong, W. B. Shi, and X. M. Wang, "Damge and failure characteristic of karst fractured rock mass under uniaxal compression," *Journal of Engineering Geology*, vol. 28, pp. 1–13, 2020.

[49] B. Li, Z. Feng, G. Z. Wang, and W. Wang, "Processes and behaviors of block topple avalanches resulting from carbonate slope failures due to underground mining," *Environmental Earth Sciences*, vol. 75, no. 8, 2016.